Construction and Building Materials 485 (2025) 141900

Contents lists available at ScienceDirect

Construction and Building Materials

journal homepage: www.elsevier.com/locate/conbuildmat

Evaluation of the durability of structural concrete with low contents of Raw-Crushed Wind Turbine Blade

Nerea Hurtado-Alonso [a,c], Miguel Bravo [b,c], Jorge de Brito [b,c], Víctor Revilla-Cuesta [d], Marta Skaf [a,*]

[a] Department of Construction, Escuela Politécnica Superior, University of Burgos, c/ Villadiego s/n, Burgos 09001, Spain
[b] Department of Civil Engineering, Architecture and Environment, Instituto Superior Técnico, University of Lisbon, Av. Rovisco Pais 1, Lisbon 1049-001, Portugal
[c] CERIS-ICIST, Instituto Técnico Superior, University of Lisbon, Av. Rovisco Pais 1, Lisbon 1049-001, Portugal
[d] Department of Civil Engineering, Escuela Politécnica Superior, University of Burgos, c/ Villadiego s/n, Burgos 09001, Spain

ARTICLE INFO

Keywords:
Raw-crushed wind turbine blade (RCWTB)
Concrete
Durability
Thermal conductivity
Shrinkage
Environmental impact

ABSTRACT

The raw crushing of wind turbine blades that have reached the end of their service life has led to the emergence of a waste material known as Raw-Crushed Wind Turbine Blade (RCWTB). Its heterogeneous composition primarily consists of fibres of glass fibre-reinforced polymer (GFRP), polymeric and balsa wood particles. This study explores the incorporation of RCWTB at low contents in concrete mixes, with a focus on its effects on durability. To this end, four concrete mixes were prepared with RCWTB contents of 0 %, 0.5 %, 1.25 %, and 2.5 %. After fresh-state and strength characterization, the mixes were evaluated for water absorption, chloride penetration resistance, carbonation resistance, thermal conductivity and shrinkage. In terms of slump and compressive strength, the incorporation of RCWTB resulted in moderate reductions in both properties. Nonetheless, all mixes reached 28-day strength values widely exceeding 30 MPa, meeting structural performance criteria. Water absorption, chloride penetration, and carbonation depth increased with RCWTB content due to the presence of porous particles within RCWTB, reaching a maximum at 1.25 % RCWTB, then stabilizing for 2.5 % RCWTB. Conversely, thermal conductivity decreased with RCWTB content due to the low-density particles of balsa wood, also stabilizing beyond 1.25 % RCWTB. All these properties followed a logarithmic evolution with the RCWTB content. Finally, the stiffness provided by GFRP fibres when incorporating 1.25 % and 2.5 % of RCWTB slightly reduced concrete shrinkage. These durability findings allow identifying potential fields of application of concrete containing low RCWTB amounts, such as façade cladding elements, interior beams and columns of buildings, or pavements.

1. Introduction

In pursuit of Europe's ambitious 2050 climate targets, which aim at a net-zero greenhouse gas emissions society [1], the rapid expansion of renewable energy sources has become essential. Within this framework, the wind energy has proven to be one of the most economically viable renewable energy sources, largely due to Europe's extensive wind resources [2]. In 2020, the wind energy sector contributed with 15 % of Europe's total energy production [3]. Furthermore, wind energy is one of the fastest-growing renewable electricity sources on the continent, with projections suggesting that wind farms could meet up to 50 % of Europe's electricity demand in the coming decades [3].

However, the rapid and large-scale expansion of this industry generates substantial waste, primarily in the form of wind turbines that reach the end of their operational life. Wind turbine blades are generally decommissioned after approximately 20–25 years of use [3], although their operational period may be extended if they continue to meet the required mechanical standards. However, in most instances, decommissioned blades are replaced by newer, more efficient models with greater power output. While much of the turbine structure, around 82 %, mainly concerning the metallic components, is recyclable [4], the blades recycling presents a significant challenge. These blades are constructed from composite materials, which complicates recycling processes due to their heterogeneous composition. Current projections by WindEurope estimate that, by 2030, Europe could face up to 350,000 tonnes of waste from decommissioned wind turbine blades alone [3]. Managing this

* Corresponding author.
E-mail address: mskaf@ubu.es (M. Skaf).

https://doi.org/10.1016/j.conbuildmat.2025.141900
Received 25 February 2025; Received in revised form 25 April 2025; Accepted 19 May 2025
Available online 23 May 2025

volume of composite waste presents an urgent challenge, underscoring the need for innovative recycling solutions to support sustainable industry growth and resource management.

The primary material required for manufacturing wind turbine blades is Glass Fibre-Reinforced Polymer (GFRP) [5]. This composite material is formed by approximately 65 % reinforcing glass fibres and 35 % polymer matrix, typically using either epoxy or polyester as the polymer [5]. Both active turbines and decommissioned units have utilized GFRP as the main structural material, with carbon fibre-reinforced polymer employed to a lesser extent [3]. The selection of these materials is based on their advantageous properties, notably a high strength-to-weight ratio, which meets the demanding aerodynamic and mechanical requirements of turbine blades, as well as providing excellent fatigue, corrosion and thermal conductivity resistance [6]. However, these thermoset composites are challenging to recycle after turbine decommissioning. Additionally, blade composition can vary depending on the manufacturer, containing elements of balsa wood and different polymers, which further complicates recycling efforts [6].

In the pursuit of an optimal recycling process for the recovery of wind turbine blades, the primary objective is to identify a method that preserves the mechanical properties of the recovered material. Current research has mainly focused on three main approaches: mechanical recycling [7,8], chemical methods like solvolysis [9–11], and thermal procedures, such as pyrolysis [12]. Each of these presents notable limitations, including high energy demands, significant CO_2 emissions, and, critically, the degradation of the mechanical properties of the recovered fibres [13]. Nevertheless, mechanical recycling, in contrast to pyrolysis and solvolysis, offers the advantage of not requiring prior separation of the blade components (GFRP, balsa wood, and polymers) [14]. The resulting material is a heterogeneous mix of particles of varying sizes, predominantly composed of the primary constituents of the blades, such as fibres from GFRP.

Based on the existing literature, recent efforts by the scientific community have been directed towards mechanically recovering this material while preserving its mechanical properties. This shredded recycled material holds considerable potential for application in the production of fibre-reinforced composites for the construction industry [15]. For instance, *Fu et al.* [16] investigated the incorporation of recycled GFRP strips, derived from the cutting of wind turbine blades, into concrete mixes. Their findings indicated a progressive reduction in workability as the proportion of recycled material increased, which was attributed to the extensive surface area of the fibres. This characteristic significantly reduced the amount of free water available within the cement matrix. However, in some cases [15], enhancements in fresh performance were observed when the loss in workability was mitigated through the addition of superplasticizers. Similarly, Yazdanbakhsh *et al.* [17] observed analogous effects when replacing the coarse aggregate fraction with between 5 % and 10 % of recycled GFRP fibres. This substitution resulted in notable reductions in slump values, further corroborating the hypothesis that the fibres' high surface area imposes an increased water demand on the cementitious system. Moreover, their study revealed that the mechanical performance of the mixes was adversely affected, with reductions in compressive strength ranging from 9 % to 15 %, depending on the GFRP incorporation level [17]. Thus, Mastali *et al.* [18] found that the stitching effect provided by the fibres was insufficient to offset these strength losses. The studies also emphasized the significant influence of the size of the recovered GFRP fibres on the strength values [15], particularly at higher material proportions.

From the perspective of analysing the durability of concrete incorporating GFRP derived from wind turbine blades, the current literature is notably limited. Existing studies have identified that both the incorporation process and the intrinsic characteristics of the fibres can have a substantial impact on the durability of the resulting concrete mixes [19]. Specifically, the addition of recycled GFRP materials has been shown to increase the porosity of concrete [20], which can lead to reductions in the resistance to the entry of external harmful agents into concrete. Furthermore, the water absorption capacity of cementitious composites increased as the proportion of recycled material rose, necessitating modifications to the mix design to balance the water-to-cement (w/c) ratio to reduce concrete porosity. With regard to shrinkage behaviour, investigations revealed a notable reduction [21], largely attributed to the role of microfibres in mitigating shrinkage during the curing process [22,23]. This beneficial effect was found to be amplified by higher levels of recycled GFRP incorporation. This gap therefore highlights the necessity of directing research efforts towards a comprehensive evaluation of durability-related properties.

This study explores the incorporation of Raw-Crushed Wind Turbine Blade (RCWTB) into concrete mixes and evaluates its effects on both mechanical properties and durability. RCWTB, a heterogeneous composite primarily consisting of GFRP, epoxy resins, polymers, and balsa wood particles derived from the non-selective mechanical crushing of decommissioned wind turbine blades, presents a complex material composition that poses unique challenges to its incorporation into cementitious systems. The incorporation of RCWTB introduces not only fibrous elements but also treated organic and polymeric fractions, each contributing distinctively to the mechanical behaviour and durability characteristics of the resulting concrete mixes. While the impact of RCWTB on compressive strength has been previously reported by the authors of this document [24], this research expands the scope by offering an in-depth examination of the durability properties of such concrete mixes.

Four concrete mixes were prepared for this study. The first served as a reference, containing 0 % RCWTB material, while the other three incorporated RCWTB at low-content levels of 0.5 %, 1.25 %, and 2.5 %. These mixes were analysed in detail in terms of mechanical performance and water absorption, along with their resistance to carbonation and chloride penetration, thermal conductivity and shrinkage. According to this approach, the novelty of this research can be summarized in the following points:

- First, the durability of concrete made with RCWTB in the terms described is evaluated, an aspect not addressed so far in the literature according to the authors' knowledge. The aim is to obtain a comprehensive overview of the durability performance of concrete made with this waste;
- Second, the addition of low RCWTB contents to concrete is also analysed for the first time. These low contents were chosen as a starting point to initiate the study of the durability of concrete with RCWTB, thus establishing the basis for advancing to the addition of higher contents of this waste to concrete in future durability research;
- Finally, by focusing on the effects of RCWTB on concrete durability, this study provides fresh insights into the durability-related viability of concrete mixes containing this waste.

2. Materials and methods

2.1. Materials

2.1.1. Cement, admixtures and water

An Ordinary Portland Cement (OPC) type CEM I 42.5 R, in accordance with European standards [25], was used. This cement was produced by Secil© (Lisbon, Portugal) and was characterized by a clinker content of 98 %. According to the supplier, this cement had a real density of approximately 3.1 Mg/m^3 , a loss on ignition of less than 5 %, an insoluble residue of less than 5 %, a sulphate (SO_3) content of less than 4 %, and a chloride content of less than 0.1 %. Its 28-day compressive strength ranged between 42.5 MPa and 62.5 MPa. Finally, its initial setting time was greater than 60 minutes and its expansion was less than 10 mm.

Concrete was prepared using potable water from the municipal water

supply system of Lisbon, Portugal, where the research was conducted. Additionally, two types of admixtures, a high-range water reducer (20HE) and a superplasticizer (5970), were used specifically in a ratio of 1:2 by weight to compensate for the loss of workability due to the incorporation of RCWTB material, ensuring acceptable slump values in a short period of time after their addition without affecting the resulting strength [24]. Both admixtures were supplied by SIKA©.

2.1.2. Aggregates

For the concrete production process, natural aggregate with a continuous size distribution across various size fractions was employed, as detailed in Fig. 1. The coarse fractions consisted of limestone in two fraction sizes, 12/22 mm and 4/12 mm, while the fine aggregate comprised siliceous river sand with particle size distributions of 1/4 mm and 0/1 mm. The complete physical properties of the aggregates are provided in Table 1, with measurements conducted in accordance with EN standardized procedures [25]: saturated surface dry density, 24-hour water absorption, bulk density, and Los Angeles abrasion resistance.

2.1.3. Raw-crushed wind turbine blade (RCWTB)

The material referred to as RCWTB was obtained by non-selectively crushing rectangular panels extracted during the decommissioning of wind turbine blades. These panels, measuring between 20 and 30 cm, were processed using a knife mill, resulting in a composite material consisting primarily of GFRP fibres, balsa wood, and polymers. The heterogeneous nature of the material obtained after the non-selective crushing process is represented in Fig. 2. The composition of the RCWTB is further detailed in Fig. 3, where fibres are identified as the predominant constituent, representing 66.80 % of the total weight [24]. In addition, 13.80 % of the material corresponded to microfibres generated during the crushing process. The physical and mechanical characterization of RCWTB revealed a global density of 1.63 kg/dm^3 and a bulk density of 246.64 kg/m^3 [26]. The low global density value of the material is attributed to the inherently low densities of its main components, including fibres (2.04 kg/dm^3) and balsa wood particles (0.33 kg/dm^3). Furthermore, the average length of the GFRP fibres was determined to be 13.1 mm, underscoring their potential role as reinforcing elements in composite applications. Further details about the production and characterisation of RCWTB can be found in a previous publication [26].

Table 1
Physical properties of each aggregate fraction according to EN standards [25].

Physical property	Aggregate fraction			
	Limestone 12/22 mm	Limestone 4/12 mm	Siliceous sand 1/4 mm	Siliceous sand 0/1 mm
Saturated surface dry density (kg/m^3)	2638.26	2641.92	2598.54	2591.15
Water absorption 24 h (% wt.)	1.50	1.25	0.66	0.31
Bulk density (kg/m^3)	1360.00	1350.27	1540.00	1530.00
Los Angeles coefficient (% wt.)	27.82	26.45	-	-

Fig. 2. RCWTB material.

2.2. Mix design

Four concrete mixes were prepared following the mix compositions specified in Table 2. The initial mix, labelled *WR0*, served as reference with an RCWTB content of 0 %. The subsequent mixes included incremental additions of RCWTB at levels of 0.5 %, 1.25 %, and 2.5 %, respectively, designated as *W0.5*, *W1.25*, and *W2.5*. These low RCWTB contents were selected to limit the proportion of particles of balsa wood in this first study on the durability of concrete containing RCWTB. These particles could be counterproductive for the durability features analysed

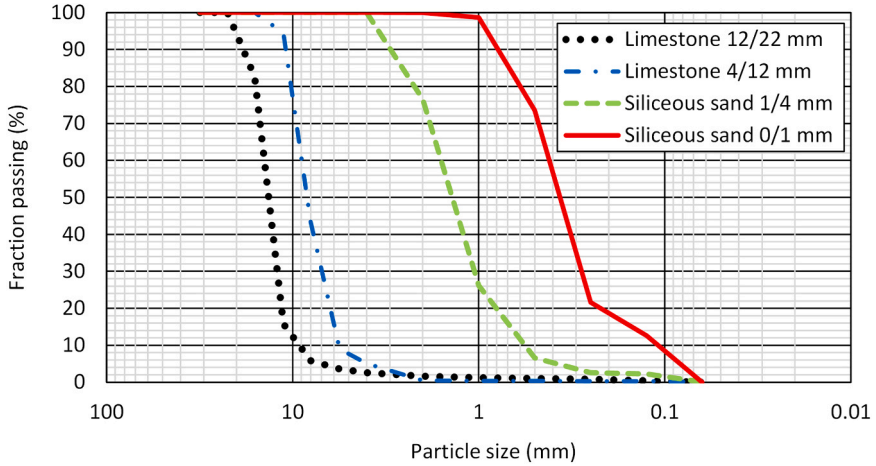

Fig. 1. Particle grading of the aggregates.

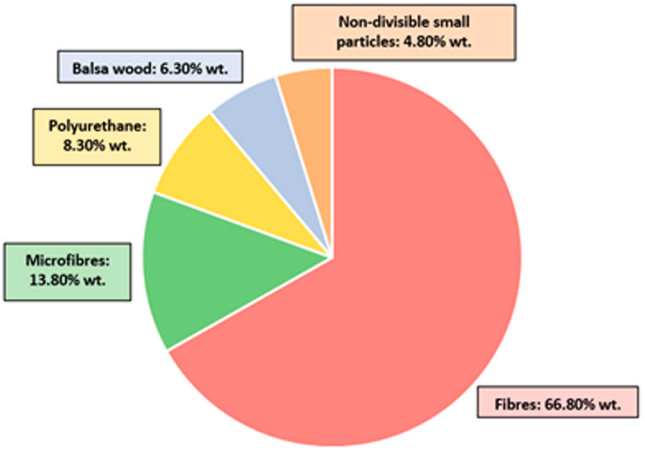

Fig. 3. Composition of RCWTB in percentage by mass.

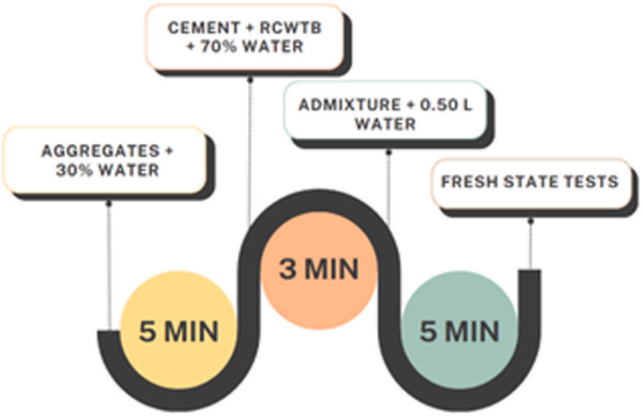

Fig. 4. Three-stage mixing process.

Table 2
Mix compositions (kg/m^3).

Mix component	*WR0*	*W0.5*	*W1.25*	*W2.5*
Cement	320	320	320	320
Plasticizer 1 (20 HE)	1.10	1.17	1.28	1.45
Plasticizer 2 (5970)	2.20	2.35	2.57	2.94
Water	153	153	153	153
Limestone 12/22 mm	715	715	715	715
Limestone 4/12 mm	405	405	405	405
Siliceous sand 1/4 mm	395	395	395	395
Siliceous sand 0/1 mm	490	490	490	490
RCWTB	0	8	20	41

[27], so in this first study it was decided to conservatively evaluate the effect of low RCWTB contents to then make decisions on higher contents to be evaluated in future research based on the obtained results. A constant cement content of 320 kg/m^3 was maintained for all mixes, along with a fixed w/c ratio of 0.48. To achieve suitable workability across all formulations, the content of both admixtures was progressively increased in proportion to the RCWTB content.

2.3. Mixing process

To ensure the proper incorporation of materials from the blades into the concrete mixes, a controlled, three-stage mixing process was followed using a horizontal-axis concrete mixer. In the initial stage, all aggregate fractions were combined with 30 % of the total water specified in the mix design. Following a five-minute mixing period in the concrete mixer, the appropriate amount of RCWTB for each mix, alongside the cement and the remaining 70 % of water, was added. The final stage commenced three minutes later, during which both superplasticizers were incorporated. Concrete was then mixed for additional five minutes to ensure homogeneity prior to fresh-state testing. Fig. 4 presents a flow diagram of the concrete mix preparation process.

2.4. Experimental campaign

As outlined in this study, the fresh-state properties of the concrete mixes were assessed immediately following fabrication, with specific measurements of slump and fresh density. For hardened-state properties, a series of specimens were prepared according to the standard requirements of each test. Table 3 presents a comprehensive summary of the tests conducted and the standards followed, including the age at testing, detailed specifications of each specimen used, and the number of samples taken for each assessment. This facilitated the calculation of mean values for each measured property, ensuring robust statistical representation of the data. Finally, analyses through Scanning Electron Microscopy (SEM) using a JEOL JSM-6460LV equipment were also conducted in the *W2.5* mix.

Table 3
Fresh-state and hardened-state tests performed according to standards.

Test	*Age of the concrete (days)*	*Specimen type*	*Number of samples*	*Standard*
Workability	Fresh concrete	-	-	EN 12350–2 [28]
Fresh density	Fresh concrete	-	-	EN 12350–6 [29]
Compressive strength	7, 28	150x150x150-mm cube specimen	2, 3	EN 12390–3 [30]
Ultrasonic pulse velocity	7, 28	150x150x150-mm cube specimen	2, 3	EN 12504–4 [31]
Immersion water absorption	28	100x100x100-mm cube specimen	2	LNEC E394 [32]
Carbonation resistance	28 + (7, 14, 28)	100Ømmx40-mm cylindrical specimen	3, 3, 3	LNEC E391 [33]
Chloride penetration resistance	28	100Ømmx50-mm cylindrical specimen	3	LNEC E463 [34]
Thermal conductivity	28	100x100x500-mm prismatic specimen	2	ISOMET 2114 [35]
Shrinkage	1–28	100x100x500-mm prismatic specimen	2	LNEC E398 [36]

24 hours after casting, the required specimens were demoulded and subsequently stored in a controlled moist chamber set at 95 ± 5 % relative humidity and 20 ± 2 °C until reaching the designated testing age. Shrinkage specimens, however, were immediately transferred to a dry chamber under conditions of 45 ± 5 % relative humidity and 20 ± 2 °C. The specimens for the evaluation of the resistance to carbonation and chloride penetration were stored in the same dry chamber starting at 14 days of age. This storage protocol ensured consistent curing and environmental exposure across all samples, facilitating accurate assessment of concrete performance properties.

2.4.1. Immersion water absorption

The immersion water absorption test was conducted following the LNEC E394 standard [32]. At 28 days of age, two cubic specimens were placed in a container, which was gradually filled with water to fully

submerge the specimens (1/3 of the height per hour). After 7 days of immersion, the saturated mass of the specimens (m_1) was measured. Subsequently, the hydrostatic mass of the saturated specimens (m_2) was determined. Finally, the specimens were dried in a ventilated oven at 105 ± 5 °C until a constant mass was achieved, and the dry mass (m_3) was recorded after 7 days. The water absorption value was calculated using Eq. (1):

$$Water\ absorption[\%] = \frac{m_1 - m_3}{m_1 - m_2} \times 100 \quad (1)$$

2.4.2. Carbonation resistance

The carbonation resistance test was conducted following the guidelines outlined in LNEC E391 [33]. Fourteen days after casting, three 100Ømmx200-mm cylindrical specimens were sectioned to yield three samples per cylinder, each measuring 4 cm in thickness and 10 cm in diameter. Then, each sample was washed and stored in a dry chamber until 28 days, age at which the samples were transferred to a carbonation chamber (CO_2 concentration of 5.0 ± 0.1 %). At 27 days, an insulating paint was applied, thus CO_2 exclusively penetrating through the lateral surfaces. After 7, 14, and 28 days of CO_2 exposure, three samples were retrieved and split into four parts, their fractured surfaces being sprayed with phenolphthalein (Fig. 5). Eight measures of the carbonation depth were recorded per surface, the result being their mean value.

2.4.3. Chloride penetration resistance

This experiment was carried out in accordance with LNEC E463 [34]. Three cylindrical concrete specimens were cut into smaller samples, each measuring 10 cm in diameter and 5 cm in height, 14 days after concrete was produced. Subsequently, the samples were rinsed with water and stored in a dry chamber until 27 days. The samples were then placed in a vacuum container at a pressure from 10 to 50 mbar for three hours. After that period, the container was filled with a saturated Ca$(OH)_2$ solution for a further hour. Then, the pressure was normalized, and the samples remained in contact with the Ca$(OH)_2$ solution for 18 ± 2 hours.

Once removed from the vacuum chamber, the samples were transferred to the migration test apparatus, which was set up with an anodic (0.3 N NaOH) and a cathodic solution (10 % of NaCl). A direct current of 30 V was applied across the samples, and the current intensity was measured. The initial and final temperatures of the anodic solution were also measured. All these aspects are illustrated in Fig. 6a. The samples were then removed from the migration apparatus, rinsed, and split in half. A silver nitrate solution was applied to the fractured surfaces, and the depth of chloride penetration was measured, as shown in Fig. 6b. Finally, the chloride migration coefficient under non-steady-state conditions (D_{nssm}) was calculated using Eq. (2).

$$D_{nssm} = \frac{0.0239 \times (273 + T) \times L}{(U - 2) \times t} \times \left(x_d - 0.0238 \times \sqrt{\frac{(273 + T) \times L \times x_d}{U - 2}} \right) \quad (2)$$

In this equation, T represents the average value of the initial and final temperature in the anolyte solution, L the thickness of the specimen, U the absolute value of the applied voltage, and x_d the average value of the penetration depth.

2.4.4. Thermal conductivity

The experiment was conducted using the ISOMET 2114 measuring device [35]. The measurements were conducted through a surface probe on the shrinkage specimens. This test was carried out in a dry chamber at 28 days of age. Two measurements were taken at a frequency range of 0.3–3 W/m·K on each sample.

2.4.5. Shrinkage

Shrinkage test was performed following LNEC E398 standard [36]. After demoulding, prismatic specimens were placed in a controlled dry chamber. Two metallic pads were attached to one lateral surface of each specimen (Fig. 7), positioned 10 cm from each. An initial reference measurement was taken 30 minutes post-demoulding using a precision shrinkage measurement device (±1 μm). During the first two weeks of the test, length measurements were conducted daily to capture early-age shrinkage behaviour. In the subsequent two weeks, measurements were taken twice weekly.

Fig. 5. Carbonation test samples.

3. Results

3.1. Fresh-state properties

The corresponding tests were conducted to evaluate the slump and fresh density of each concrete mix. The primary objective was to analyse the influence of incorporating RCWTB on these properties, given that the presence of GFRP fibres significantly reduces both workability and density [37,38].

The slump tests (Table 4) indicated a slump value of 60 mm for the reference mix (*WR0*), which fell within the S2 slump class (50–90 mm). As the proportion of RCWTB increased, a significant reduction in slump was observed, dropping from 60 mm to just 10 mm for the mix with the highest RCWTB content. The least pronounced decrease occurred with the incorporation of only 0.5 % RCWTB, where the slump value was reduced from 60 mm to 50 mm. For mixes with 1.25 % RCWTB or more, the workability appeared to stabilize at a minimum value of 10 mm. This behaviour is primarily attributed to the morphology of the RCWTB particles, which are irregular due to the stochastic nature of the crushing process [39,40]. The angular and rough texture of the crushed waste increases internal friction and inhibits the movement of coarse aggregate particles within the concrete matrix [41,42]. At higher RCWTB proportions, this texture further hindered the flow of the coarse aggregates through the mix, causing segregation of these particles from the rest of the matrix and leading to a loss in workability [43]. The w/c ratio was maintained constant throughout the whole study, which ensured uniformity in the mix design across all experimental formulations, but it likely amplified the observed reduction in workability. Furthermore, minor increases in the quantity of superplasticizers were necessary to

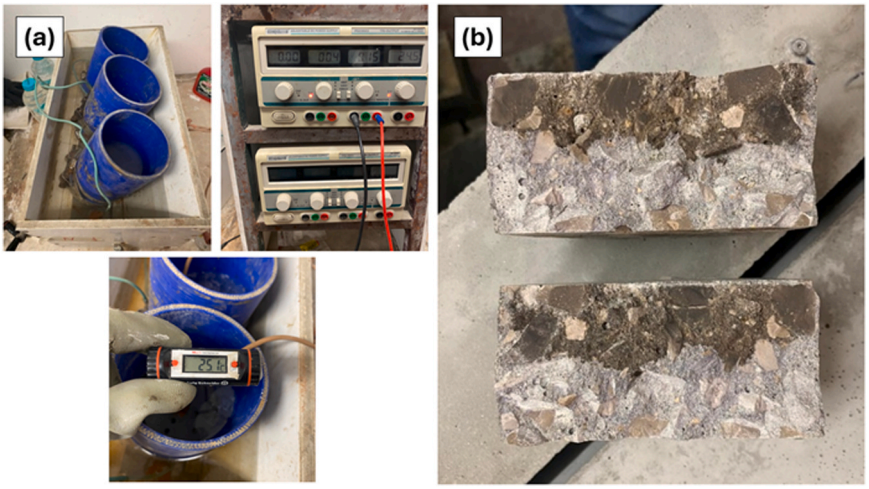

Fig. 6. (a) Elements of the chloride penetration test in progress; (b) depth of the chloride penetration in the fracture surfaces of a specimen.

Fig. 7. Prismatic specimens for shrinkage test.

Table 4
Slump values and fresh density of the mixes.

Mix	Slump (mm)	Fresh density (kg/m^3)
WR0	60	2383.11
W0.5	50	2358.52
W1.25	10	2306.07
W2.50	10	2349.33

partly counteract the loss of fluidity at a constant w/c ratio [44]. However, these adjustments inadvertently resulted in the fresh-state improvement of concrete for such RCWTB contents.

The fresh density values, summarized in Table 4, also decreased as RCWTB was incorporated. The reference mix (*WR0*) exhibited the highest density (2383.11 kg/m^3), which was expected, as it did not contain any additional materials that could affect compaction or introduce air voids. With the incorporation of the waste, the density decreased by up to 1.42 % for the mix with the maximum RCWTB content (*W2.5*) compared to the reference mix. Interestingly, the greatest reduction (3.23 %) was observed in the mix containing 1.25 % RCWTB. These variations, while not highly significant, can be explained by the presence of components with lower densities than those used in regular concrete production, such as balsa wood and polymer particles [45].

3.2. Hardened state properties

3.2.1. Compressive strength

Compressive strength tests were conducted on the concrete mixes at 7 and 28 days of curing (Fig. 8 and Table 5). At both curing ages, the measured compressive strength consistently exceeded 25 MPa, proving the structural viability of concrete with RCWTB. These findings indicate that the addition of RCWTB does not adversely impact the compressive strength of concrete in terms of suitability for structural applications [46].

The incorporation of increasing RCWTB contents in the mixes revealed a clear trend of decreasing compressive strength at both curing ages evaluated. The reference mix (*WR0*) consistently exhibited the highest compressive strength values at 7 and 28 days, while the mix with

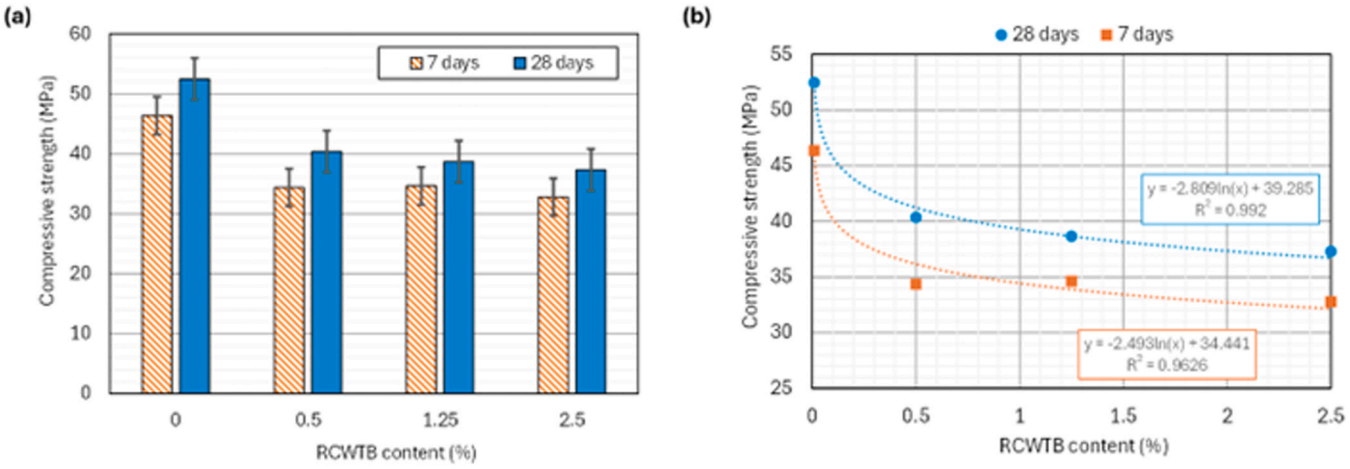

Fig. 8. Compressive strength evaluation at 7 and 28 days of age: (a) overall values; (b) analysis of the relationship between RCWTB content and compressive strength values.

Table 5
Compressive strength values at 7 and 28 days of age and strength evolution over time.

Mix	Compressive strength at 7 days (MPa)	Compressive strength at 28 days (MPa)	Δ7–28 days (%)
WR0	46.35 ± 1.17	52.47 ± 0.64	88.34
W0.5	34.36 ± 0.13	40.37 ± 1.24	85.11
W1.25	34.64 ± 0.13	38.67 ± 0.97	89.58
W2.5	32.78 ± 1.66	37.31 ± 0.58	87.86

the highest RCWTB content (2.50 %) showed the lowest values, with reductions of approximately 29 % at both ages. This reduction is primarily due to the presence of fibres, which absorb a portion of the water. As a result, less water remains available for the cement hydration process, potentially affecting the strength development of the resulting material. Although the GFRP fibres present in RCWTB provided a stitching effect to the cementitious matrix, their contribution was insufficient to fully counterbalance such an adverse effect. Furthermore, the presence of weak particles such as polymer and balsa wood within the RCWTB further hindered proper bonding with the cement matrix, intensifying the reduction in compressive strength [47].

Despite these reductions, mixes incorporating RCWTB displayed relatively similar compressive strength values across the different RCWTB content levels. This trend is consistent with previous research findings [48]. The reduction in strength between the mix with 0.50 % RCWTB and the one with 2.50 % RCWTB was quantified as 1.58 MPa at 7 days and 3.06 MPa at 28 days, representing less than 1 % in both cases. The increased presence of GFRP fibres within the RCWTB at higher content levels mitigated the strength losses, preventing them from being as pronounced as those observed between the reference mix (*WR0*) and the 0.50 % RCWTB mix (*W0.5*). This beneficial stitching effect of GFRP fibres was particularly evident at the early curing age of 7 days. At this stage, the reductions in strength for each incremental increase in RCWTB content were less pronounced. This can be attributed to the higher deformability of the cementitious matrix during the initial curing period, which allowed the GFRP fibres to effectively enhance structural integrity by bridging micro-cracks and improving load transfer within the matrix [49]. Furthermore, RCWTB did not affect the evolution of strength over time, as can be noted from the fourth column of Table 5.

The logarithmic models developed to explain the relationship between compressive strength and RCWTB incorporation at both curing ages are depicted in Fig. 8b. At 28 days of age, the slope in logarithmic scale of the trend line (-2.809) indicated a reduction in compressive strength as RCWTB content increased. A similar trend was observed at 7 days, though the slope was less steep (-2.493), demonstrating that the impact of RCWTB on compressive strength was less significant at earlier ages. The coefficients of determination (R^2) for the models were exceptionally high, at 0.9626 and 0.9920 for the 7-day and 28-day curing periods, respectively, confirming that the logarithmic relationship accurately describes the observed trends. The use of a logarithmic function to model this relationship highlights the non-linear impact of RCWTB on compressive strength. Instead of a constant decline, the data reveal that the initial increments of RCWTB had a more pronounced effect, while at higher levels of incorporation the impact diminished. This behaviour can be interpreted as a saturation effect: at lower RCWTB levels, the material interacts more actively with the mix components, leading to significant reductions in strength [50]. However, as the RCWTB content increases further, its effects become less pronounced.

Fig. 9 provides a visual representation of the damage sustained under compressive loading for cubic specimens from mixes with the lowest and highest RCWTB content, as depicted in Fig. 9a and Fig. 9b, respectively. The specimen corresponding to the reference mix (Fig. 9a) displayed significant visible crushing and deformation under load, indicative of a lack of internal reinforcement to resist crack propagation. In contrast, the specimens containing RCWTB (Fig. 9b) demonstrated significantly enhanced integrity, both at early ages and after 28 days, compared to the reference mix. The addition of RCWTB fibres appeared to mitigate cracking, contributing to the preservation of the specimen's structural integrity. For the *W2.5* mix, only fine vertical cracks were observed along the loading axis. This behaviour can be attributed to the presence of GFRP fibres, which acted as a stitching mechanism within the matrix, as a SEM analysis confirmed. In Fig. 10, a GFRP fibre of the *W2.5* mix is shown, which was perfectly embedded in the cementitious matrix and bonded to it, as evidenced by the tiny fragments of matrix adhered to its

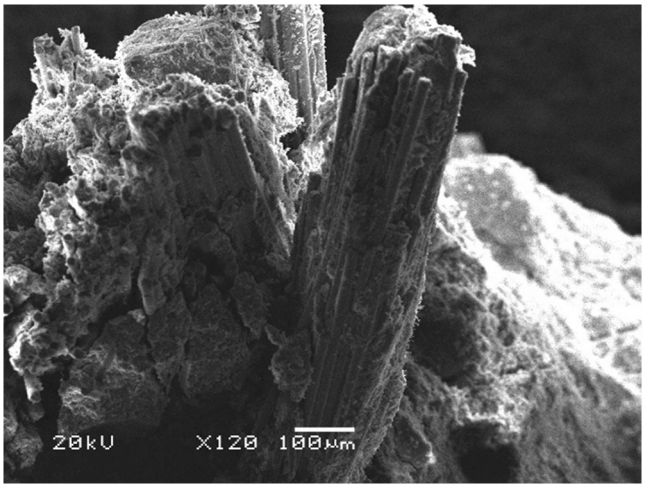

Fig. 10. SEM image of a GFRP fibre in the *W2.5* mix.

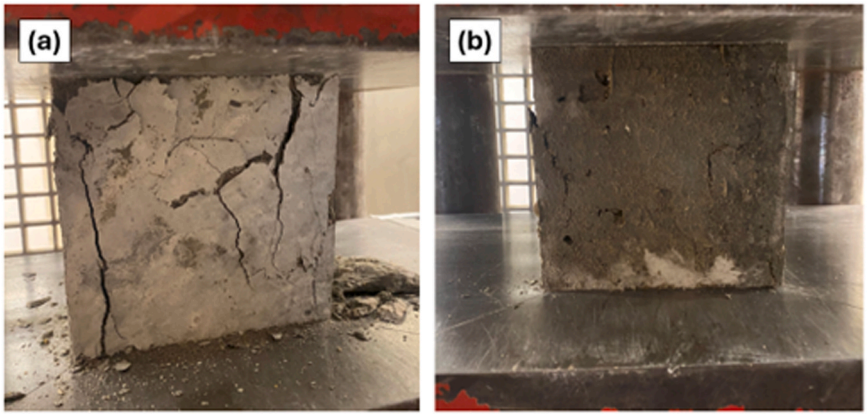

Fig. 9. Compressive damage of the cubic specimens at the age of 28 days: (a) *WR0*; (b) *W2.5*.

surface after slippage due to compressive loading. Globally, the RCWTB material provided a bridging mechanism, effectively stitching cracks and preventing the detachment of concrete fragments following failure [51]. This phenomenon became increasingly pronounced as the RCWTB content in the mix increased, indicating a correlation between the fibre content and the material's ability to resist fragmentation under compression [52].

3.2.2. Ultrasonic pulse velocity and dynamic modulus of elasticity

The Ultrasonic Pulse Velocity (UPV) test was conducted at 7 and 28 days, and its values are presented in Fig. 11a. The results of the dynamic modulus of elasticity, calculated through the obtained UPV values [53], are depicted in Fig. 11b.

Regarding UPV, all measured values were within the acceptable range of 4.7–5.2 km/s [54]. The incorporation of RCWTB resulted in a slight decrease in velocity, with a reduction of 0.41 km/s observed between the reference mix and the 2.5 % RCWTB mix after 7 days. At this early stage, the presence of RCWTB appears to hinder the propagation of ultrasonic waves. This may be attributed to the interference caused by the fibres and low-density particles present in RCWTB, which potentially disrupt the uniform transmission of the waves [24,55]. However, this effect diminished with the concrete age, with a marked improvement observed at 28 days compared to 7 days of age. At this later age, the impact of the waste on wave propagation becomes negligible, and the recorded velocities are even slightly higher than those of the reference mix. This demonstrates the quality of the concrete matrix reached when using RCWTB as a component in concrete mixes [56]. While initially its incorporation may introduce minor impediments to wave transmission, these effects decrease over time, ultimately resulting in a stable and effective material suitable for application in concrete. Finally, the small error bars indicated minimal dispersion in the data, reflecting high measurement consistency.

The dynamic modulus of elasticity calculated from the UPV measurements did not show large variations, with all the mixes exhibiting a value slightly higher than 50 GPa. The particles of balsa wood and polymers contained in RCWTB have a higher deformability and lower density than the natural aggregate. Consequently, the incorporation of such components in concrete when RCWTB is added diminishes the static modulus of elasticity of concrete according to previous studies [24]. However, it seems that this effect was fully counterbalanced under dynamic conditions by the GFRP fibres, which stitched the cementitious matrix and in turn increased elastic stiffness [37]. Thus, the dynamic modulus of elasticity remained constant regardless of the amount of RCWTB added.

3.3. Durability tests

3.3.1. Water absorption

The water absorption test by immersion was conducted to evaluate the water absorption capacity of the various concrete mixes. The results are presented in Fig. 12a, which shows the water absorption values for each mix. A general upward trend in water absorption was observed as the RCWTB content increased. The reference mix exhibited the lowest value of 9.14 %, while the highest value, 9.87 %, was recorded for the *W1.25* mix. The remaining mixes displayed water absorption values of 9.66 % (*W0.5*) and 9.73 % (*W2.5*), supporting the conclusion that the incorporation of RCWTB undoubtedly increased the water absorption capacity of concrete.

Statistical analysis of the relationship between water absorption values and RCWTB incorporation (Fig. 12b) revealed a logarithmic fit with a coefficient of determination (R^2) of 0.9182. The trend of the logarithmic curve was upward upon the incorporation of RCWTB. This behaviour can be attributed to the increased porosity of the cementitious matrix and the existence of particles within the RCWTB, such as balsa wood and polymer particles, which exhibit significantly higher porosity than natural aggregate [27]. However, two exceptional observations emerged from the general trend that warrant further discussion:

- Mix *W0.5*: Although the water absorption value for the mix containing 0.5 % RCWTB was higher than that of the reference mix, the increase was only around 6 %. This finding suggests that at low RCWTB content levels, the barrier effect of GFRP fibres within the waste mitigates the negative effects of porous materials [57], such as balsa wood and polymer particles, making RCWTB addition viable without significant detriment to water absorption capacity;
- Mix *W2.5*: Interestingly, the *W1.25* mix exhibited a higher water absorption than the *W2.5* mix. This indicates that the influence of increasing RCWTB content on water absorption stabilized at levels from 1.25 % to 2.5 %. Similarly to the behaviour observed with the 0.5 % RCWTB mix, the fibres in RCWTB contribute to reducing water absorption, counteracting the effects of porous components [57].

3.3.2. Carbonation resistance

The influence of RCWTB addition on the carbonation resistance of the concrete mixes was evaluated. Fig. 13a presents the carbonation depth of concrete mixes with varying percentages of RCWTB addition, measured after exposure to CO_2 for 7, 14, and 28 days.

The results indicate a progressive increase in carbonation depth over time, from 7 to 14 and then to 28 days, underscoring the significant role of exposure duration in the carbonation process. This behaviour aligns with the diffusion-controlled mechanism of CO_2 uptake that governs

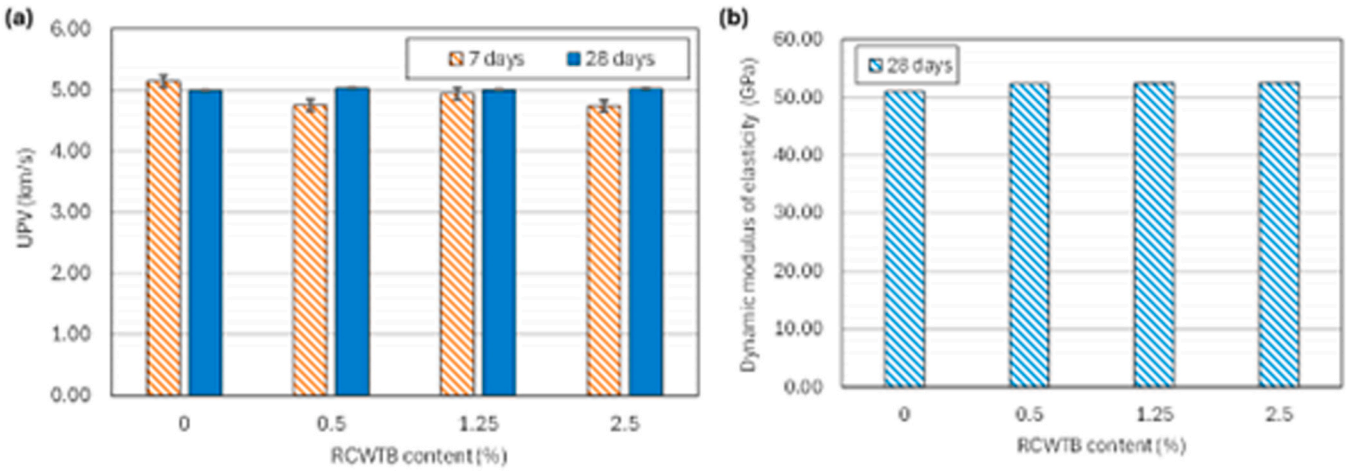

Fig. 11. UPV evaluation at 7 and 28 days of age: (a) UPV results; (b) 28-day dynamic modulus of elasticity.

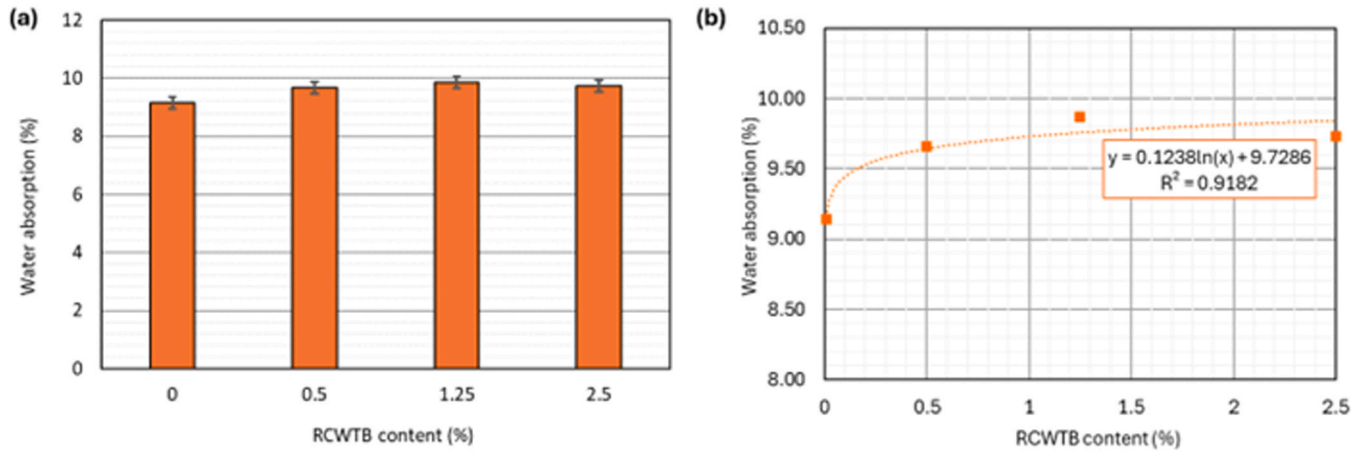

Fig. 12. Variations of the water absorption values for different RCWTB content: (a) effect of RCWTB content on the water absorption; (b) analysis of the relationship between RCWTB content and water absorption.

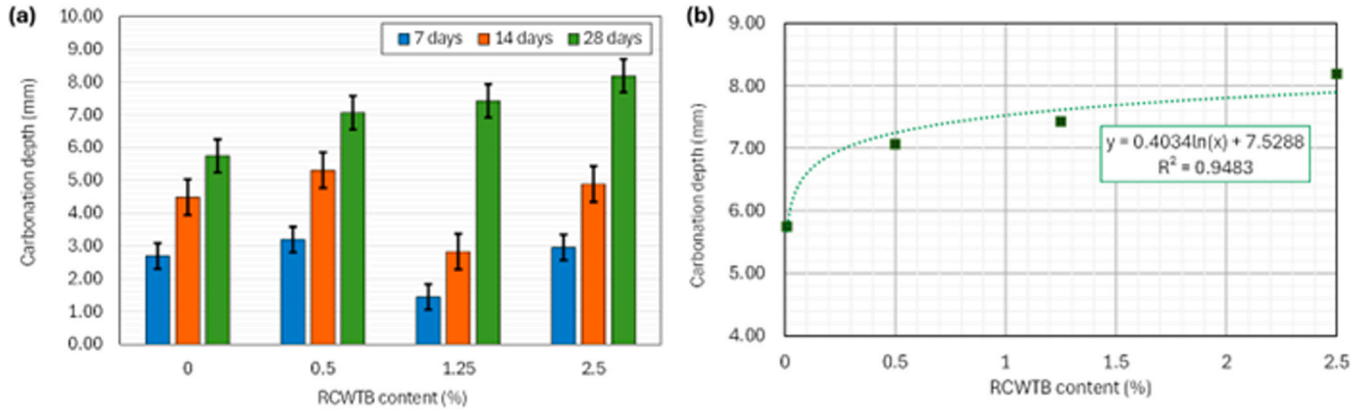

Fig. 13. Carbonation depth of the concrete mixes with RCWTB after 7, 14 and 28 days of CO_2 exposition: (a) overall values; (b) analysis of the linear regression at 28 days of age.

carbonation reactions, which becomes more pronounced with prolonged exposure periods [58].

However, the relationship between RCWTB content and carbonation depth is not strictly the same for all exposure periods. At 7 and 14 days, the highest carbonation depth was observed for a 0.5 % RCWTB addition, rather than higher percentages. Specifically, at 7 days, the mix with 2.5 % RCWTB exhibited a 10 % increase in carbonation depth compared to the reference mix (*WR0*), while the mix with 0.5 % RCWTB showed a more significant increase of 19 %. Interestingly, the mix containing 1.25 % RCWTB demonstrated a marked 46 % reduction in carbonation depth relative to *WR0*. At 14 days, a similar trend was observed: carbonation depth increased by 8 % for *W2.5* and 18 % for *W0.5*, whereas *W1.25* experienced a 37 % decrease compared to *WR0*. This performance can once again be attributed to the beneficial effect of the GFRP fibres and their opposition to the CO_2 spreading within the concrete for low exposure times when added in such amount, as found in concrete produced with other types of fibres [59,60]. At 28 days, however, the trend shifted, with carbonation depth increasing consistently with RCWTB content. Specifically, increments of 23 %, 29 %, and 43 % were observed for *W0.5*, *W1.25*, and *W2.5*, respectively.

The relationship between RCWTB content and carbonation depth at 28 days was modelled using a logarithmic function, which provided an excellent fit to the experimental data ($R^2 = 0.9483$). Additionally, error bars in the experimental data indicate moderate variability, likely due to experimental inconsistencies or material heterogeneity. The logarithmic model (Fig. 13b) revealed a decelerating growth pattern: carbonation depth increases rapidly at low RCWTB contents (0–0.5 %) but stabilizes progressively at higher contents (1.25 % and 2.5 %). This behaviour might be attributed to the increased permeability caused by the reduced cohesion of the weak particles in the RCWTB to the concrete matrix [61,62], which facilitates CO_2 diffusion and consequently eases carbonation depth when the resistance mechanism of the GFRP fibres detected for low exposure times is already overcome [45]. Despite the overall increase in carbonation depth with the addition of RCWTB, its effect decreased from 1.25 % RCWTB onwards, and the increase of carbonation depth for this and higher RCWTB amounts was lower than that recorded between the *WR0* and *W0.5* mixes. This performance suggests a saturation limit in the material's ability to influence carbonation [50].

3.3.3. *Chloride penetration resistance*

The chloride penetration resistance of the concrete was evaluated at 28 days of age, and the results for the non-steady state migration coefficients are presented in Fig. 14a. The migration coefficients increased with the RCWTB waste content, with the lowest value observed in the reference mix (14.39×10^{-12} m^2/s). In comparison, the mix with the highest RCWTB content exhibited an increase of up to 69 %, reaching a diffusion coefficient of $24.30 \times 10^{-1\ 2}$ m^2/s.

Migration coefficients for RCWTB contents of 0.5 %, 1.25 %, and 2.5 % were significantly higher than those of the mix without waste (*WR0*). This result suggests that the addition of RCWTB increased the ionic permeability or facilitated the migration of substances through concrete over time. The observed increase in migration coefficients can

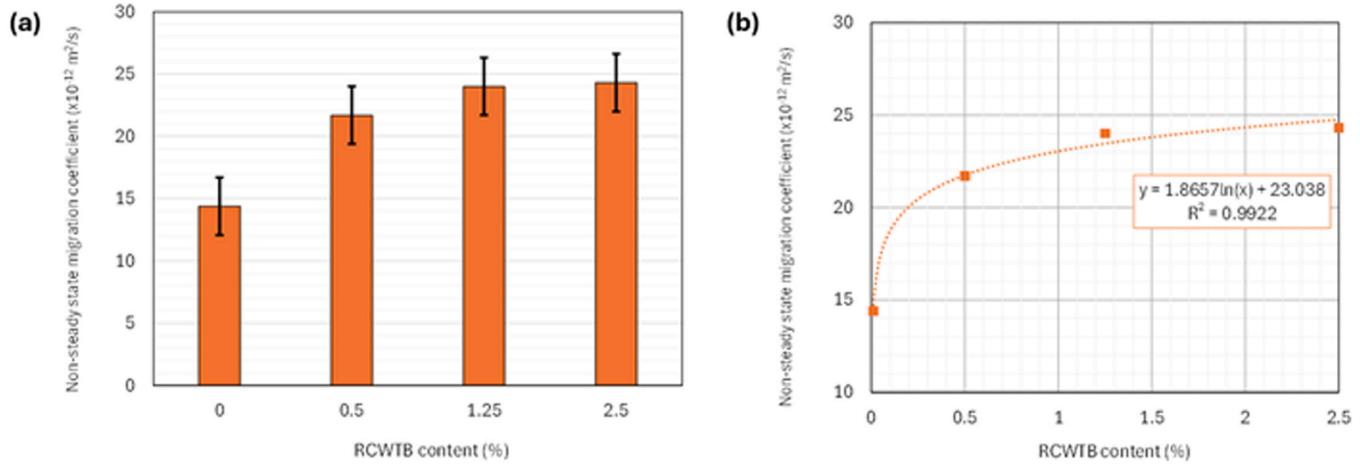

Fig. 14. Non-steady state migration coefficient of RCWTB mixes at 28 days: (a) effect of RCWTB content on chloride migration coefficient; (b) analysis of the relationship between RCWTB content and chloride migration coefficient.

be attributed to microstructural alterations induced by the incorporation of RCWTB, which likely resulted in increased porosity and reduced density within the mix [63]. This heightened porosity reduces the material's overall density and consequently diminishes its resistance to chloride penetration [47]. Such changes in the microstructure may facilitate the transport of chloride ions, thereby reducing the durability and protective capacity of concrete. Furthermore, the most notable increase occurred at lower RCWTB concentrations: between 0 % and 0.5 %, the migration coefficient showed a substantial rise, whereas the increase became less pronounced at higher concentrations (1.25 % to 2.5 %), with only a 1 % additional increment.

The analysis revealed a logarithmic trend in the increase of chloride ion penetration in concrete as the RCWTB content increased, as illustrated in Fig. 14b. The logarithmic model demonstrated a strong correlation ($R^2 = 0.9922$), indicating excellent predictive capability. The curve exhibited a rapid increase initially (from 0 % to 0.5 % RCWTB) but gradually decelerated as the RCWTB content rose. This behaviour suggests that the initial effect of RCWTB was more pronounced, but its marginal influence diminished at higher concentrations.

The error bars indicated moderate dispersion; nevertheless, the differences between RCWTB levels were consistent. Overall, RCWTB had a negative impact on the chloride migration coefficient, although this effect tended to stabilize at higher RCWTB contents (from 1.25 % to 2.5 %). The strong correlation of the logarithmic model further supports its suitability for predicting the material's performance at various RCWTB contents.

3.3.4. *Thermal conductivity*

Fig. 15a illustrates the influence of RCWTB addition on the thermal conductivity (λ) of different concrete mixes at 28 days of age. It revealed a significant reduction in thermal conductivity as the RCWTB content increased. The reference concrete (*WR0*) exhibited the highest thermal conductivity, with a value of 2.32 W/(m·K). However, incorporating RCWTB reduced the thermal conductivity by up to 19 %. This decrease was most pronounced in the initial increments of RCWTB content, stabilizing beyond 0.5 %, where variations became minimal (approximately 1 % for contents greater than 0.5 %). For example, the thermal conductivity at 0.5 % RCWTB was 1.88 W/(m·K), while at 1.25 % and 2.5 % RCWTB, it remained relatively constant at 1.90 W/(m·K).

This behaviour suggests that RCWTB acts as a poor thermal conductor, making it a suitable material for thermal insulation applications. The reduction in thermal conductivity is likely attributable, first, to the presence of fibres and particles of balsa wood in RCWTB, which introduces voids that cannot be fully filled by the cement paste [27]. Additionally, the overall density of the mix decreases with RCWTB addition, further contributing to lower thermal conductivity [63]. Finally, materials such as balsa wood and polymeric particles typically exhibit lower heat transfer capacity [64].

The results for thermal conductivity are also consistent with those found in the water absorption analysis, where an increased number of

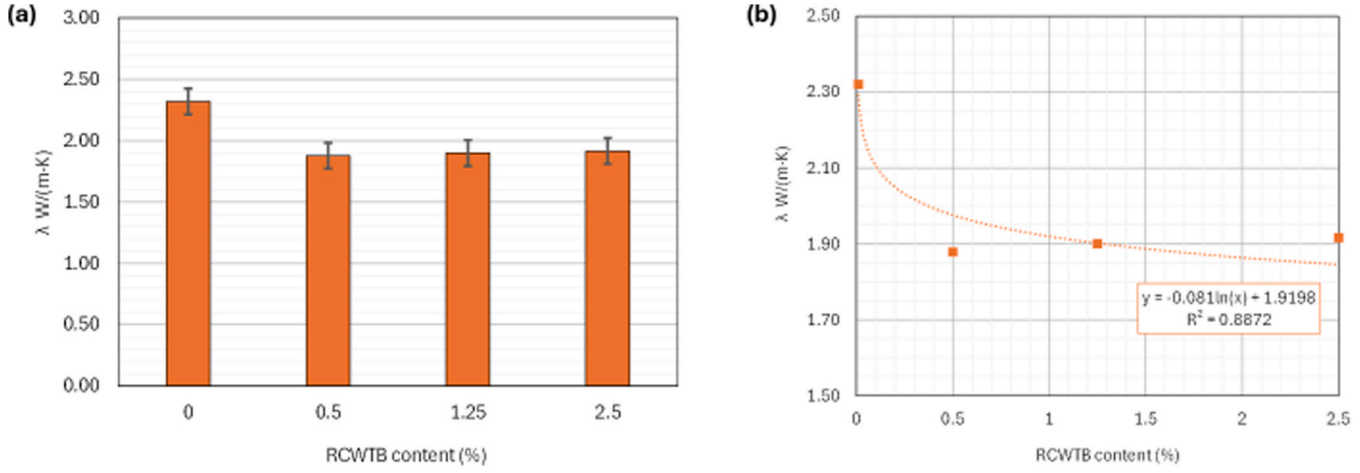

Fig. 15. Thermal conductivity of the concrete mixes at 28 days of age: (a) overall values; (b) analysis of the relationship between RCWTB content and thermal conductivity.

voids corresponded to higher absorption levels. These voids, in turn, reduce the material's thermal conductivity, as evidenced by earlier studies [65,66].

The error bars in Fig. 15a indicate that the differences in thermal conductivity values are consistent and statistically significant. The reduction in such property with increasing RCWTB contents follows a non-linear trend: the most significant impact occurs between 0 % and 0.5 % RCWTB, while additional reductions at higher RCWTB levels are marginal. This behaviour is well-represented by a logarithmic curve (Fig. 15b) with a coefficient of determination (R^2) of 0.8872, indicating a reasonable, though less precise, fit compared to other properties.

3.3.5. Shrinkage

The variation of shrinkage over time for the four mixes is presented in Fig. 16. All mixes exhibited a significant increase in shrinkage during the first 7 days, followed by a reduced rate of shrinkage between days 7 and 28, as indicated by a lower slope. At 28 days, shrinkage almost stabilized. This behaviour is typical of cementitious materials, where the early-stage shrinkage is primarily driven by rapid moisture loss [64].

The reference mix (*WR0*) demonstrated a lowest shrinkage throughout the whole testing period than the mix with 0.5 % RCWTB content (*W0.5*). This trend suggests that low RCWTB content led to greater shrinkage, which can be attributed to higher porosity and reduced density and stiffness in the concrete's microstructure [67]. These structural modifications, caused by the presence of components such as balsa wood and polymeric particles, increase the susceptibility of the material to volumetric contraction as moisture is lost, and counterbalance the positive effect of the GFRP fibres [65]. However, 7 days after casting, the shrinkage values for mixes *WR0*, *W1.25* and *W2.5* were 0.103, 0.105 and 0.095 mm/m, respectively. Furthermore, between days 7 and 28, the shrinkage of the mixes *W1.25* and *W2.5* increased at a slower pace compared to the *WR0* mix, thus their 28-day shrinkage results being 0.188, 0.162 and 0.161 mm/m. It is clear that the GFRP fibres, acting as rigid elements within the concrete matrix [68], were more effective in reducing shrinkage for RCWTB contents from 1.25–2.5 %.

The drying shrinkage data over time were successfully modelled using logarithmic fits (Fig. 16), with most mixes showing high accuracy in the adjustment. The shrinkage behaviour can be divided into two distinct phases [68], accurately represented through logarithmic models:

- Early stage (0–7 days): Characterized by a steep slope in the shrinkage curve, indicating rapid water loss during the initial hydration and curing process;
- Later stage (7–28 days): Marked by a slower shrinkage rate as the water loss diminishes and the material approaches stabilization.

3.4. Overall analysis

Fig. 17 shows a radar graph in which all the durability properties analysed in this research are presented. As each durability property had different units, for this representation all the properties were normalized considering that 1 was the maximum value of the property recorded among all the mixes and 0 a null property value.

This overall analysis of the properties firstly shows that the addition of low contents of RCWTB slightly affected the durability of concrete regarding the penetration of harmful external agents. Second, the addition of 1.25 % and 2.5 % RCWTB to concrete led to very similar results regarding water absorption, carbonation and chloride penetration. Finally, any RCWTB content improved thermal conductivity, while 1.25 % and 2.5 % RCWTB reduced shrinkage. Therefore, potential applications of concrete with low RCWTB amounts from a durability approach could be façade cladding elements due to the improved thermal insulation and proper resistance to the penetration of harmful external agents [69]; interior beams and columns of buildings because of the suitable durability yielded with up to 2.5 % RCWTB [70]; and pavements, in which shrinkage limitation is important [71]. These initial approaches need to be verified with more targeted research and pilot testing.

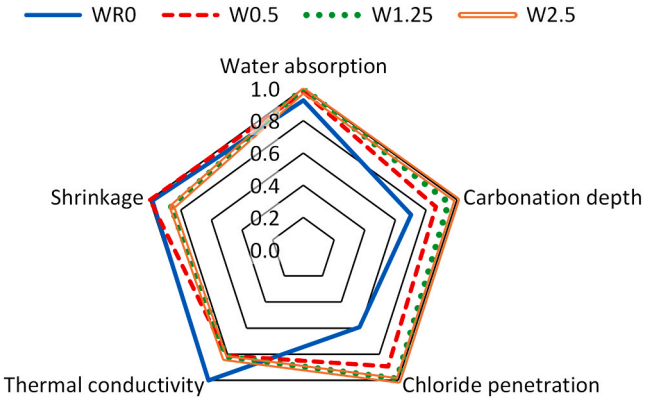

Fig. 17. Radar graph of the durability properties of concrete with low contents of RCWTB.

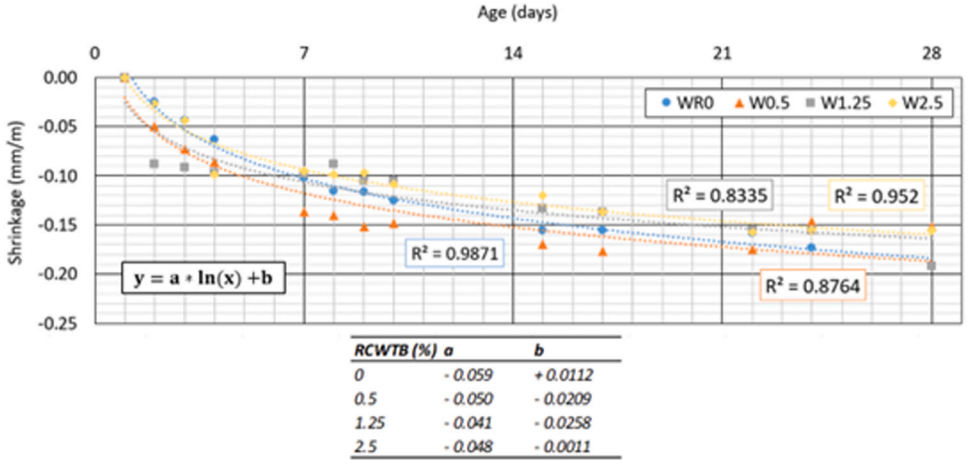

RCWTB (%)	a	b
0	- 0.059	+ 0.0112
0.5	- 0.050	- 0.0209
1.25	- 0.041	- 0.0258
2.5	- 0.048	- 0.0011

Fig. 16. Shrinkage of concrete mixes with RCWTB content.

4. Conclusions

This study investigated the influence of incorporating a waste material from the raw crushing of dismantled wind turbine blades, known as Raw-Crushed Wind Turbine Blade (RCWTB), into concrete mixes, mainly focusing on the durability aspects of the resulting mixes. Several concrete formulations were prepared with low RCWTB contents ranging from 0 % to 2.5 %. The key findings of this research can be summarized as follows:

- The incorporation of RCWTB into concrete did not undermine its structural integrity, as all mixes widely exceeded 25 MPa at both 7 and 28 days. While a reduction in compressive strength was observed with increasing RCWTB contents, this decrease was partially mitigated by the presence of GFRP fibres, particularly at early ages, thus following a logarithmic evolution as a function of the RCWTB content. Additionally, UPV measurements showed a slight decrease at 7 days due to the interference of fibres and mainly low-density particles, but by 28 days, the differences in UPV were minimal;

- In terms of durability, all evaluated properties (water absorption, carbonation depth, and chloride penetration) exhibited a clear logarithmic trend with the RCWTB content at 28 days. The incorporation of RCWTB resulted in a deterioration of the material's behaviour, with this effect becoming more pronounced as the RCWTB content increased. Nevertheless, this trend stabilized at 1.25 % RCWTB content, suggesting that the presence of GFRP fibres effectively counteracted the detrimental effects of the other components in RCWTB;

- With respect to carbonation resistance, the addition of RCWTB affected this property in a time-dependent manner. At 7 and 14 days, concrete mixes with lower RCWTB contents (0.5 %) exhibited a greater carbonation depth than when adding 1.25 % and 2.5 % RCWTB. GFRP fibres exhibited a beneficial effect for such RCWTB amounts, thus partially counteracting CO_2 diffusion within short exposure times;

- The addition of RCWTB substantially reduced the thermal conductivity of concrete, particularly at lower RCWTB contents (from 0 % to 0.5 %), where the greatest relative reduction in conductivity was observed. This reduction stabilized at higher RCWTB proportions, showing only marginal variations. This decrease, modelled by a logarithmic curve, was attributed to the increased porosity and lower density of concrete due to the incorporation of balsa wood and polymer particles within RCWTB. These materials acted as poor thermal conductors, making concrete containing this waste an effective candidate for thermal insulation applications;

- RCWTB also led to a decrease in concrete shrinkage when added from an amount of 1.25 %. The GFRP fibres helped partially stiffen the cementitious matrix, mainly hindering its contraction at the later stages (7–28 days). In fact, lower shrinkage levels than those of the reference concrete (0 % RCWTB) were reached. However, the deformability of the particles of polymers and balsa wood increased shrinkage when incorporating 0.5 % RCWTB in concrete. Shrinkage followed a logarithmic pattern with concrete age.

5. Limitations and future lines of research

In conclusion, this study on the incorporation of low contents of RCWTB as a component in concrete mixes yielded promising insights into its effect on various durability-related properties of concrete. However, this research has only addressed the effect of low RCWTB contents, obtained from a specific type of wind turbine blade, at the standard concrete age of 28 days. Furthermore, the environmental and economic implications of the use of low contents of this waste in concrete have not been addressed. Thus, the following future research lines can be envisaged to gain a comprehensive understanding of how RCWTB affects concrete durability performance over time and its potential applications in construction materials:

- It is crucial to explore the implications of the use of this material in concrete when it is produced from blades of different types and origins, as RCWTB composition and characteristics may vary;
- Future research should also focus on evaluating durability properties at advanced ages and when adding higher amounts of this waste in concrete;
- Other durability properties, such as water and gas permeability or fire resistance should also be analysed;
- Finally, life cycle assessment of concrete with these low RCWTB amounts should be conducted. Accurate estimations of the production cost of RCWTB and, consequently, of concrete with low RCWTB contents, should also be addressed. So, a more comprehensive approach to the use of this waste in concrete would be obtained, as existing studies regarding other wastes demonstrate [72,73].

CRediT authorship contribution statement

Nerea Hurtado-Alonso: Conceptualization, Formal analysis, Investigation, Methodology, Software, Validation, Writing – original draft. **Miguel Bravo:** Conceptualization, Formal analysis, Investigation, Methodology, Software, Validation, Visualization, Writing – review & editing. **Jorge de Brito:** Conceptualization, Formal analysis, Investigation, Methodology, Software, Validation, Visualization, Writing – review & editing. **Víctor Revilla-Cuesta:** Conceptualization, Formal analysis, Investigation, Methodology, Software, Validation, Visualization, Writing – review & editing. **Marta Skaf:** Conceptualization, Funding acquisition, Methodology, Project administration, Resources, Supervision, Writing – review & editing.

Declaration of Competing Interest

The authors declare that they have no known competing financial interests or personal relationships that could have appeared to influence the work reported in this paper.

Ackowledgements

This research work was supported by the Spanish Ministry of Universities, MICIU, AEI, EU, ERDF and NextGenerationEU/PRTR [grant numbers PID2023–146642OB-I00; 10.13039/501100011033; TED2021–129715B-I00]; the Junta de Castilla y León (Regional Government) and ERDF [grant number UIC-231; BU033P23; BU066–22]; and the University of Burgos [grant number SUCONS, Y135.GI]. The authors also acknowledge the support of the Foundation for Science and Technology, through funding UIDB/04625/2020, CERIS Research Centre and Instituto Superior Técnico. Open access funding provided by University of Burgos

Data Availability

Data will be made available on request.

References

[1] European Parliament, The European green deal, Off. J. Eur. Union 64 (2020).
[2] N. Tazi, J. Kim, Y. Bouzidi, E. Chatelet, G. Liu, Waste and material flow analysis in the end-of-life wind energy system, Resour. Conserv Recycl 145 (2019) 199–207, https://doi.org/10.1016/j.resconrec.2019.02.039.
[3] F. Spini, P. Bettini, End-of-Life wind turbine blades: Review on recycling strategies, Compos Part B Eng. 275 (2024) 111290, https://doi.org/10.1016/j.compositesb.2024.111290.

[4] L. Allekotte, P. Garrett, Life Cycle Assessment of electricity production from an offshore V236–15 MW wind plant, 2024. ⟨https://www.vestas.com/en/sustainability/environment/lifecycle-assessments⟩.
[5] J.P. Jensen, K. Skelton, Wind turbine blade recycling: experiences, challenges and possibilities in a circular economy, Renew. Sust. Energy Rev. 97 (2018) 165–176, https://doi.org/10.1016/j.rser.2018.08.041.
[6] M. Schmid, N. Gonzalez, A. Dierckx, T. Wegman, Accelerating Wind Turbine Blade Circularity, 2020.
[7] S.J. Pickering, Recycling technologies for thermoset composite materials—current status, Compos Part A Appl. Sci. Manuf. 37 (2006) 1206–1215, https://doi.org/10.1016/j.compositesa.2005.05.030.
[8] J. Beauson, H. Lilholt, P. Brøndsted, Recycling solid residues recovered from glass fibre-reinforced composites – A review applied to wind turbine blade materials, J. Reinform. Plast. Comp. 33 (2014) 1542–1556, https://doi.org/10.1177/0731684414537131.
[9] S. Utekar, S. V K, N. More, A. Rao, Comprehensive study of recycling of thermosetting polymer composites – driving force, challenges and methods, Compos Part B Eng. 207 (2021) 108596, https://doi.org/10.1016/j.compositesb.2020.108596.
[10] S. Gharde, B. Kandasubramanian, Mechanothermal and chemical recycling methodologies for the Fibre Reinforced Plastic (FRP), Environ. Technol. Innov. 14 (2019) 100311, https://doi.org/10.1016/j.eti.2019.01.005.
[11] G. Oliveux, J.L. Bailleul, E.L.G.La Salle, Chemical recycling of glass fibre reinforced composites using subcritical water, Compos Part A Appl. Sci. Manuf. 43 (2012) 1809–1818, https://doi.org/10.1016/j.compositesa.2012.06.008.
[12] M. Rani, P. Choudhary, V. Krishnan, S. Zafar, A review on recycling and reuse methods for carbon fiber/glass fiber composites waste from wind turbine blades, Compos Part B Eng. 215 (2021) 108768, https://doi.org/10.1016/j.compositesb.2021.108768.
[13] S. Karuppannan Gopalraj, T. Kärki, A review on the recycling of waste carbon fibre/glass fibre-reinforced composites: fibre recovery, properties and life-cycle analysis, SN Appl. Sci. 2 (2020) 433, https://doi.org/10.1007/s42452-020-2195-4.
[14] Z. Pu, S. Yang, Q. Wang, Recycling of waste wind turbine blades for high-performance polypropylene composites, J. Appl. Polym. Sci. 141 (2024) e55474, https://doi.org/10.1002/app.55474.
[15] H. Li, J. Yang, D. Yang, N. Zhang, S. Nazar, L. Wang, Fiber-reinforced polymer waste in the construction industry: a review, Environ. Chem. Lett. 22 (2024) 2777–2844, https://doi.org/10.1007/s10311-024-01769-5.
[16] B. Fu, K.C. Liu, J.F. Chen, J.G. Teng, Concrete reinforced with macro fibres recycled from waste GFRP, Constr. Build. Mater. 310 (2021) 125063, https://doi.org/10.1016/j.conbuildmat.2021.125063.
[17] A. Yazdanbakhsh, L. Bank, Y. Tian, Mechanical Processing of GFRP Waste into Large-Sized Pieces for Use in Concrete, Recycling 3 (2018) 8, https://doi.org/10.3390/recycling3010008.
[18] M. Mastali, A. Dalvand, A.R. Sattarifard, The impact resistance and mechanical properties of reinforced self-compacting concrete with recycled glass fibre reinforced polymers, J. Clean. Prod. 124 (2016) 312–324, https://doi.org/10.1016/j.jclepro.2016.02.148.
[19] J. Manso-Morato, N. Hurtado-Alonso, V. Revilla-Cuesta, M. Skaf, V. Ortega-López, Fiber-Reinforced concrete and its life cycle assessment: a systematic review, J. Build. Eng. 94 (2024) 110062, https://doi.org/10.1016/j.jobe.2024.110062.
[20] A. Dehghan, K. Peterson, A. Shvarzman, Recycled glass fiber reinforced polymer additions to Portland cement concrete, Constr. Build. Mater. 146 (2017) 238–250, https://doi.org/10.1016/j.conbuildmat.2017.04.011.
[21] B. Zhou, M. Zhang, L. Wang, G. Ma, Experimental study on mechanical property and microstructure of cement mortar reinforced with elaborately recycled GFRP fiber, Cem. Concr. Compos 117 (2021) 103908, https://doi.org/10.1016/j.cemconcomp.2020.103908.
[22] D. Židanavičius, M. Augonis, N. Adamukaitis, I.Villalon Fornes, Concrete shrinkage analysis with quicklime, microfibers, and SRA admixtures, Materials 16 (2023) 2061, https://doi.org/10.3390/ma16052061.
[23] L. Onghero, M.Tramontin Souza, D. Cusson, W. Repette, Influence of glass microfibers on the control of autogenous shrinkage in very high strength self-compacting concretes (VHSSCC), J. Comp. Sci. 8 (2024) 101, https://doi.org/10.3390/jcs8030101.
[24] V. Revilla-Cuesta, J. Manso-Morato, N. Hurtado-Alonso, M. Skaf, V. Ortega-López, Mechanical and environmental advantages of the revaluation of raw-crushed wind-turbine blades as a concrete component, J. Build. Eng. 82 (2024) 108383, https://doi.org/10.1016/j.jobe.2023.108383.
[25] EN-Euronorm, European Committee for Standardization, Rue de Stassart, 36. Belgium-1050 Brussels, 2020.
[26] V. Revilla-Cuesta, M. Skaf, V. Ortega-López, J.M. Manso, Raw-crushed wind-turbine blade: Waste characterization and suitability for use in concrete production, Resour. Conserv Recycl 198 (2023) 107160, https://doi.org/10.1016/j.resconrec.2023.107160.
[27] V. Revilla-Cuesta, F. Faleschini, C. Pellegrino, M. Skaf, V. Ortega-López, Water transport and porosity trends of concrete containing integral additions of raw-crushed wind-turbine blade, Dev. Built Environ. 17 (2024) 100374, https://doi.org/10.1016/j.dibe.2024.100374.
[28] EN-Euronorm, EN 12350-2: Testing fresh concrete Part 2: Slump test, Rue de Stassart, 36. Belgium-1050 Brussels, 2020.
[29] EN-Euronorm, EN 12350-6: Testing fresh concrete Part 6: Density, Rue de Stassart, 36. Belgium-1050 Brussels, 2020.
[30] EN-Euronorm, EN 12390-3: Testing hardened concrete. Part 3: Compressive strength of test specimens, Rue de Stassart, 36. Belgium-1050 Brussels, 2020.
[31] EN-Euronorm, EN 12504-4: Testing concrete in structures. Part 4: Determination of ultrasonic pulse velocity, Rue de Stassart, 36. Belgium-1050 Brussels, 2020.
[32] National Laboratory in Civil Engineering (LNEC), LNEC E 394. Concrete: determination of the absorption of water by immersion, Lisboa, Portugal, 1998.
[33] National Laboratory in Civil Engineering (LNEC), LNEC E 391. Concrete: determination of carbonation resistance., Lisboa, Portugal, 1993.
[34] National Laboratory in Civil Engineering (LNEC), LNEC E 463. Concrete: determination of diffusion coefficient of chlorides from non-steady state migration test, Lisboa, Portugal, 2004.
[35] ISOMET 2114. Applied Precision, Ltd.: Bratislava, Slovakia, 2010. ⟨https://www.appliedp.com/download/catalog/isomet_pc_en.pdf⟩.
[36] National Laboratory in Civil Engineering (LNEC), LNEC E 398. Concrete: Determination of Drying Shrinkage and Expansion, Lisboa, Portugal, 1993.
[37] G.T. Xu, M.J. Liu, Y. Xiang, B. Fu, Valorization of macro fibers recycled from decommissioned turbine blades as discrete reinforcement in concrete, J. Clean. Prod. 379 (2022) 134550, https://doi.org/10.1016/j.jclepro.2022.134550.
[38] A. Paktiawal, M. Alam, Alkali-resistant glass fiber high strength concrete and its durability parameters, Mater. Today Proc. 47 (2021) 4758–4766, https://doi.org/10.1016/j.matpr.2021.05.668.
[39] Y. Xiao, A. Gu, Z. Lu, Dispersion, workability and mechanical properties of different steel-microfiber-reinforced concretes with low fiber content, Sustainability 10 (2018) 2335, https://doi.org/10.3390/su10072335.
[40] T. Borhan, M. Abo Dhaheer, Z. Mahdi, Characteristics of sustainable self-compacting concrete reinforced by fibres from waste materials, Arab J. Sci. Eng. 45 (2020) 4359–4367, https://doi.org/10.1007/s13369-020-04460-3.
[41] L. Hong, X. Gu, F. Lin, Influence of aggregate surface roughness on mechanical properties of interface and concrete, Constr. Build. Mater. 65 (2014) 338–349, https://doi.org/10.1016/j.conbuildmat.2014.04.131.
[42] J.Y. Jia, X.L. Gu, Effects of coarse aggregate surface morphology on aggregate-mortar interface strength and mechanical properties of concrete, Constr. Build. Mater. 294 (2021) 123515, https://doi.org/10.1016/j.conbuildmat.2021.123515.
[43] Y. Zhao, Y. Duan, L. Zhu, Y. Wang, Z. Jin, Characterization of coarse aggregate morphology and its effect on rheological and mechanical properties of fresh concrete, Constr. Build. Mater. 286 (2021) 122940, https://doi.org/10.1016/j.conbuildmat.2021.122940.
[44] I. Bentegri, O. Boukendakdji, E.H. Kadri, T.T. Ngo, H. Soualhi, Rheological and tribological behaviors of polypropylene fiber reinforced concrete, Constr. Build. Mater. 261 (2020) 119962, https://doi.org/10.1016/j.conbuildmat.2020.119962.
[45] V. Revilla-Cuesta, A.B. Espinosa, R. Serrano-López, M. Skaf, J. Manso, Mechanical properties of concrete mixes with selectively crushed wind turbine blade: comparison with raw-crushing, Materials 17 (2024) 6299, https://doi.org/10.3390/ma17246299.
[46] Eurocode 2, Eurocode 2, Design of Concrete Structures. Part 1-1: General Rules and Rules for Buildings (EN 1992-1-1), CEN (European Committee for Standardization), 2010.
[47] C. Xu, Q. Li, P. Wang, Y. Guo, Preparation and performance research of ecological concrete using waste wood, Case Stud. Constr. Mat. 20 (2024) e03221, https://doi.org/10.1016/j.cscm.2024.e03221.
[48] J. Manso-Morato, N. Hurtado-Alonso, V. Revilla-Cuesta, V. Ortega-López, Management of wind-turbine blade waste as high-content concrete addition: mechanical performance evaluation and life cycle assessment, J. Environ. Manag. 373 (2025) 123995, https://doi.org/10.1016/j.jenvman.2024.123995.
[49] J. Wang, C. Wang, Y. Ji, R. Qie, D. Wang, G. Liu, Mechanical properties and microscopic study of recycled fibre concrete based on wind turbine blades, Materials 17 (2024) 3565, https://doi.org/10.3390/ma17143565.
[50] H. Mazaheripour, S. Ghanbarpour, S.H. Mirmoradi, I. Hosseinpour, The effect of polypropylene fibers on the properties of fresh and hardened lightweight self-compacting concrete, Constr. Build. Mater. 25 (2011) 351–358, https://doi.org/10.1016/j.conbuildmat.2010.06.018.
[51] L.A. Le, G.D. Nguyen, H.H. Bui, A.H. Sheikh, A. Kotousov, Incorporation of micro-cracking and fibre bridging mechanisms in constitutive modelling of fibre reinforced concrete, J. Mech. Phys. Solids 133 (2019) 103732, https://doi.org/10.1016/j.jmps.2019.103732.
[52] V. Berardi, Fracture failure modes in fiber-reinforced polymer systems used for strengthening existing structures, Appl. Sci. 11 (2021) 6344, https://doi.org/10.3390/app11146344.
[53] V. Revilla-Cuesta, V. Ortega-López, M. Skaf, J.M. Manso, Effect of fine recycled concrete aggregate on the mechanical behavior of self-compacting concrete, Constr. Build. Mater. 263 (2020) 120671, https://doi.org/10.1016/j.conbuildmat.2020.120671.
[54] V.M. Malhotra, Testing hardened concrete: non destructive methods (1976).
[55] S. Kumar, U. Sharma, Mechanical performance of cement concrete with use of combined fibers of basalt and bamboo, Phys. Chem. Eart Parts A/B/C. 137 (2025) 103799, https://doi.org/10.1016/j.pce.2024.103799.
[56] J. Wang, Q. Dai, R. Si, S. Guo, Mechanical, durability, and microstructural properties of macro synthetic polypropylene (PP) fiber-reinforced rubber concrete, J. Clean. Prod. 234 (2019) 1351–1364, https://doi.org/10.1016/j.jclepro.2019.06.272.
[57] M. Kumar, H. Jena, Water absorption behaviour of glass fibre-reinforced polymer composite with clamshell and cenosphere fillers, Proc. Inst. Mech. Eng., Part E: J. Proc. Mech. Eng. 238 (2022) 2061–2068, https://doi.org/10.1177/09544089221132433.
[58] H. Cui, W. Tang, W. Liu, Z. Dong, F. Xing, Experimental study on effects of CO2 concentrations on concrete carbonation and diffusion mechanisms, Constr. Build. Mater. 93 (2015) 522–527, https://doi.org/10.1016/j.conbuildmat.2015.06.007.

[59] P. Zhang, Y. Yang, S. Hu, M. Jiao, Y. Ling, Mechanical properties and durability of polypropylene and steel fiber-reinforced recycled aggregates concrete (FRRAC): a review, Sustainability 12 (2020) 9509, https://doi.org/10.3390/su12229509.
[60] Y. Li, J. Zhang, Y. He, G. Huang, J. Li, Z. Niu, B. Gao, A review on durability of basalt fiber reinforced concrete, Compos Sci. Tech. 225 (2022) 109519, https://doi.org/10.1016/j.compscitech.2022.109519.
[61] M. Ramli, W.H. Kwan, N.F. Abas, Strength and durability of coconut-fiber-reinforced concrete in aggressive environments, Constr. Build. Mater. 38 (2013) 554–566, https://doi.org/10.1016/j.conbuildmat.2012.09.002.
[62] S. Luhar, I. Luhar, D. Nicolaides, R. Gupta, Durability Performance Evaluation of Rubberized Geopolymer Concrete, Sustainability 13 (2021) 5969, https://doi.org/10.3390/su13115969.
[63] H. Harabi, M.L.K. Khouadjia, S. Bensalem, H.F. Isleem, M. Khishe, Effect of waste paper aggregate and polyethylene terephthalate on mortar performance, Sci. Rep. 14 (2024) 29588, https://doi.org/10.1038/s41598-024-80914-0.
[64] N. Vahedi, C. Tiago, A.P. Vassilopoulos, J.R. Correia, T. Keller, Thermophysical properties of balsa wood used as core of sandwich composite bridge decks exposed to external fire, Constr. Build. Mater. 329 (2022) 127164, https://doi.org/10.1016/j.conbuildmat.2022.127164.
[65] M. Barka, O. Taleb, A.K. Tedjditi, H. Soualhi, A.S. Benosman, M. Mouli, Impact of polypropylene fibers on the rheological, mechanical, and thermal properties of self-compacting concrete, MRS Adv. 9 (2024) 1128–1136, https://doi.org/10.1557/s43580-024-00905-1.
[66] V. Kočí, E. Vejmelková, D. Koňáková, V. Pommer, S. Grzeszczyk, A. Matuszek-Chmurowska, A. Mordak, R. Černý, Basic physical, mechanical, thermal and hygric properties of reactive powder concrete with basalt and polypropylene fibers after high-temperature exposure, Constr. Build. Mater. 374 (2023) 130922, https://doi.org/10.1016/j.conbuildmat.2023.130922.
[67] N.P. Tran, C. Gunasekara, D.W. Law, S. Houshyar, S. Setunge, A. Cwirzen, A critical review on drying shrinkage mitigation strategies in cement-based materials, J. Build. Eng. 38 (2021) 102210, https://doi.org/10.1016/j.jobe.2021.102210.
[68] N. Yousefieh, A. Joshaghani, E. Hajibandeh, M. Shekarchi, Influence of fibers on drying shrinkage in restrained concrete, Constr. Build. Mater. 148 (2017) 833–845, https://doi.org/10.1016/j.conbuildmat.2017.05.093.
[69] J. Barrelas, I.S. Dias, A. Silva, J. de Brito, I. Flores-Colen, A. Tadeu, Impact of environmental exposure on the service life of façade claddings—a statistical analysis, Buildings 11 (12) (2021) 615, https://doi.org/10.3390/buildings11120615.
[70] M. Elkafrawy, P. Gowrishankar, N.G. Aswad, A. Alashkar, A. Khalil, M. AlHamaydeh, R. Hawileh, GFRP-reinforced concrete columns: state-of-the-art, behavior, and research needs, Buildings 14 (10) (2024) 3131, https://doi.org/10.3390/buildings14103131.
[71] D. Rambabu, S.K. Sharma, M. Abdul Akbar, A review on suitability of using geopolymer concrete for rigid pavement, Inn. Infr Sol. 7 (2022) 286, https://doi.org/10.1007/s41062-022-00878-w.
[72] L. Lin, J. Xu, W. Ying, Y. Yu, L. Zhou, Post-fire compressive mechanical behaviors of concrete incorporating coarse and fine recycled aggregates, Constr. Build. Mater. 461 (2025) 139948, https://doi.org/10.1016/j.conbuildmat.2025.139948.
[73] Y. Yu, G.H. Fang, R. Kurda, A.R. Sabuj, X.Y. Zhao, An agile, intelligent and scalable framework for mix design optimization of green concrete incorporating recycled aggregates from precast rejects, Case Stud. Constr. Mat. 20 (2024) e03156, https://doi.org/10.1016/j.cscm.2024.e03156.